



# Automatic segmentation of puborectalis muscle on three-dimensional transperineal ultrasound

F. VAN DEN NOORT<sup>1,2</sup> , A. T. M. GROB<sup>1,2</sup> , C. H. SLUMP<sup>1</sup>, C. H. VAN DER VAART<sup>2</sup> and M. VAN STRALEN<sup>3</sup>

<sup>1</sup>MIRA Institute for Biomedical Technology and Technical Medicine, University of Twente, Enschede, The Netherlands; <sup>2</sup>Department of Reproductive Medicine and Gynecology, University Medical Center, Utrecht, The Netherlands; <sup>3</sup>Imaging Division, University Medical Center Utrecht, Utrecht, The Netherlands

**KEYWORDS:** 3D segmentation; active appearance model; puborectalis muscle; ultrasound

## ABSTRACT

**Objectives** The introduction of three-dimensional (3D) analysis of the puborectalis muscle (PRM) for diagnostic purposes into daily practice is hindered by the need for appropriate training of observers. Automatic segmentation of the PRM on 3D transperineal ultrasound may aid its integration into clinical practice. The aims of this study were to present and assess a protocol for manual 3D segmentation of the PRM on 3D transperineal ultrasound, and to use this for training of automatic 3D segmentation method of the PRM.

**Methods** The data used in this study were derived from 3D transperineal ultrasound sequences of the pelvic floor acquired at 12 weeks' gestation from nulliparous women with a singleton pregnancy. A manual 3D segmentation protocol was developed for the PRM based on a validated two-dimensional segmentation protocol. For automatic segmentation, active appearance models of the PRM were developed, trained using manual segmentation data from 50 women. The performances of both manual and automatic segmentation were analyzed by measuring the overlap and distance between the segmentations. Intraclass correlation coefficients (ICCs) and their 95% CIs were determined for mean echogenicity and volume of the puborectalis muscle, in order to assess inter- and intraobserver reliabilities of the manual method using data from 20 women, as well as to compare the manual and automatic methods.

**Results** Interobserver reliabilities for mean echogenicity and volume were very good for manual segmentation (ICCs 0.987 and 0.910, respectively), as were intraobserver reliabilities (ICCs 0.991 and 0.877, respectively). ICCs for mean echogenicity and volume were very good and good, respectively, for the comparison of manual vs

automatic segmentation (0.968 and 0.626, respectively). The overlap and distance results for manual segmentation were as expected, showing an average mismatch of only 2–3 pixels and reasonable overlap. Based on overlap and distance, five mismatches were detected for automatic segmentation, resulting in an automatic segmentation success rate of 90%.

**Conclusions** This study presents a reliable manual segmentation protocol and automatic 3D segmentation method for the PRM, which will facilitate future investigation of the PRM, allowing for the reliable measurement of potentially clinically valuable parameters such as mean echogenicity. © 2017 The Authors. *Ultrasound in Obstetrics & Gynecology* published by John Wiley & Sons Ltd on behalf of the International Society of Ultrasound in Obstetrics and Gynecology.

## INTRODUCTION

The levator ani muscles provide support for the pelvic organs. During vaginal delivery, trauma to these muscles will occur in one-fifth to one-third of women<sup>1,2</sup>. This trauma weakens pelvic floor support and may cause problems such as pelvic organ prolapse and urinary incontinence<sup>3,4</sup>. During delivery, the part of the levator ani muscle that surrounds the urogenital hiatus, the puborectalis muscle (PRM), has to stretch to more than twice its original length and may therefore sustain damage<sup>5,6</sup>.

It is not well understood why some women experience pelvic floor problems after delivery while others do not. Some studies suggest that it might be due to changes in muscle structure that occur during pregnancy, prior to delivery<sup>7–9</sup>. It is to be expected that these changes will be reflected in muscle functionality. Recently, in studies that used three- and four-dimensional (3D/4D)

Correspondence to: F. van Limbeek-van den Noort, University of Twente, Carre 3.526, Drienerlolaan 5, 7522NB, Enschede, The Netherlands (e-mail: f.vandennoort@utwente.nl)

Accepted: 26 September 2017

ultrasound imaging to visualize the PRM, new informative parameters of the PRM were obtained; for example, hiatal dimensions<sup>10,11</sup>, mean echogenicity of the PRM (MEP)<sup>9,12,13</sup> and strain<sup>14</sup>. Hiatal dimensions and strain are related to, and provide insight into the functionality of, the PRM. Early pregnancy MEP has been shown to be related to mode of delivery<sup>13</sup>.

However, in these studies parameters of the PRM were obtained manually, which is time-consuming, hindering their introduction into clinical practice. Sindhwani *et al.*<sup>15</sup> proposed a method to automate the measurement of hiatal dimensions. However, these are static two-dimensional (2D) measurements, not exploiting the full potential of 3D/4D ultrasound. Therefore, the aim of this work was to develop an automatic segmentation method for the PRM in 3D transperineal ultrasound images.

Active appearance models (AAMs), which require manually annotated training data, have proved to be reliable in automatically segmenting structures in 3D ultrasound (e.g. the left ventricle<sup>16</sup>). As 3D segmentation of the PRM on 3D ultrasound is, to the best of our knowledge, as yet unexplored, we present a manual 3D segmentation protocol for the PRM on 3D transperineal ultrasound. We assessed its reproducibility and used it to generate training data for an AAM. The performance of the fully automatic AAM was then analyzed by comparing it with manual segmentation.

## METHODS

### Data

The data for this study were obtained from a dataset acquired by van Veelen *et al.*<sup>17</sup> that consists of 3D/4D transperineal ultrasound data of the pelvic floor from 280 nulliparous women with a singleton pregnancy who were scanned at multiple time points pre- and postpartum. In the current study we focused on scans acquired at 12 weeks' gestation. The acquisition was performed using a GE Voluson 730 Expert system (GE Medical Systems, Zipf, Austria), equipped with a RAB 4–8-MHz curved-array volume transducer. The settings of the system were kept constant to minimize variation across acquisitions, since the main aim of this study was to investigate the MEP. The acquisition started with the PRM at rest, and then the women were asked to contract their PRM fully and, afterwards, to perform a Valsalva maneuver, which results in a stretched PRM.

A dataset of 63 videoclips was selected randomly from the original dataset. While selecting, videoclips were checked by an observer for the following inclusion criteria: the PRM is contained entirely in the field of view; the symphysis is in the field of view to allow measurement of the minimal hiatal dimensions; and image quality is sufficient. Owing to the consistent ultrasound settings, some images had poor contrast, insufficient for 3D delineation of the PRM. For the quality criterion, two observers had to agree on whether image quality was sufficient for inclusion.

Thirteen videoclips did not meet all the criteria and were discarded. Of these, five did not fully capture the PRM in 3D, five did not capture the symphysis and three were of poor image quality, thus 50 videoclips were included in the study. From each of these, one frame in which the PRM was at rest was selected. A randomly selected subset of data from 20 subjects was used to analyze the manual segmentations.

The ultrasound clips were converted to DICOM in 4D View 9.0 (GE Medical Systems). In-house developed software, based on MeVisLab 2.6.2 (MeVis Medical Solutions, Bremen, Germany)<sup>18</sup>, was used for selecting the frame with the PRM at rest, manual segmentation using splines, AAM training and AAM matching.

### 3D segmentation protocol

The 3D segmentation protocol is an extension of an existing validated protocol for 2D segmentation<sup>11,12</sup>. To ensure optimal visibility of the PRM, the protocol starts with rotating to the slice with minimal hiatal dimensions (SMHD) (Figure 1c)<sup>10</sup>, which allows browsing through the tomographic ultrasound images<sup>19</sup>.

2D segmentation of the PRM in the SMHD has been presented previously<sup>12</sup>, and is shown in Figure 1c. In slices close to the SMHD, the segmented shape of the PRM

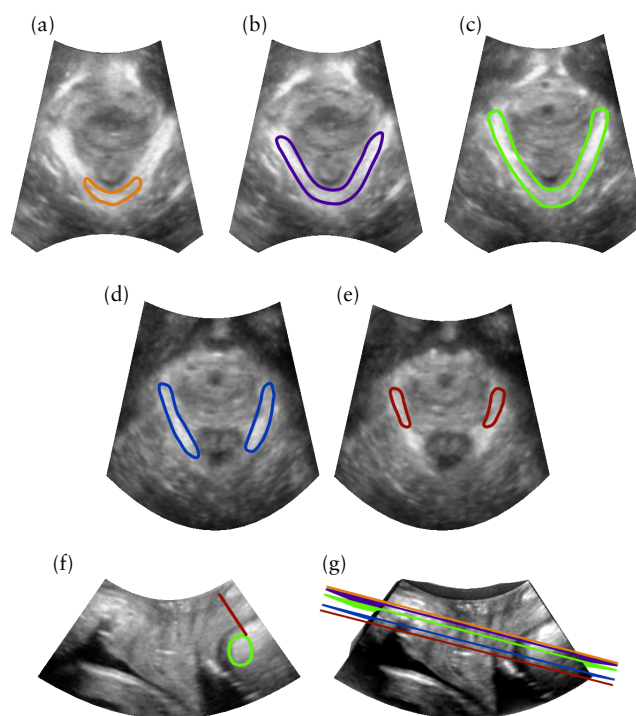


**Figure 1** Manual three-dimensional segmentation on transperineal ultrasound of puborectalis muscle (PRM) (delineated) in different axial slices, from caudal to cranial, showing: (a) caudal limit of PRM; (b) slice in which PRM is disconnected visually from pubic symphysis; (c) slice of minimal hiatal dimensions; (d) slice in which posterior part of PRM is out-of-plane; (e) cranial limit of PRM; (f) segmentation of PRM in midsagittal slice, with green line showing how to determine boundary between external anal sphincter and PRM; and (g) position of slices (a)–(e) on midsagittal slice.

is the same as in the SMHD; however, the segmented shape changes in slices further away. Caudal from the SMHD, the segmented shape of the PRM is detached visually from the symphysis, as shown in Figure 1b. The distance between the segmented area and the symphysis will increase further, moving to the caudal limit of the PRM. This caudal limit (Figure 1a) is found by using the midsagittal plane (Figure 1f), in which the distinction between the PRM and the external sphincter is much clearer than in the axial view.

Cranial from the SMHD, the posterior part of the PRM will disappear (Figure 1d). So from here, the PRM needs to be segmented as two separate parts. It is hard to determine the cranial boundary of the PRM. However, Singh *et al.*<sup>20</sup> showed that there is sharp angulation between the PRM and the iliococcygeus muscle. Therefore, the last cranial slice is the one before the PRM becomes indistinguishable from its surroundings or before the areas that appear to be part of the PRM start moving outwards (Figure 1e).

### Active appearance model

AAMs model the typical variation in shape and texture of an object presented in training data<sup>21</sup>. When the manual

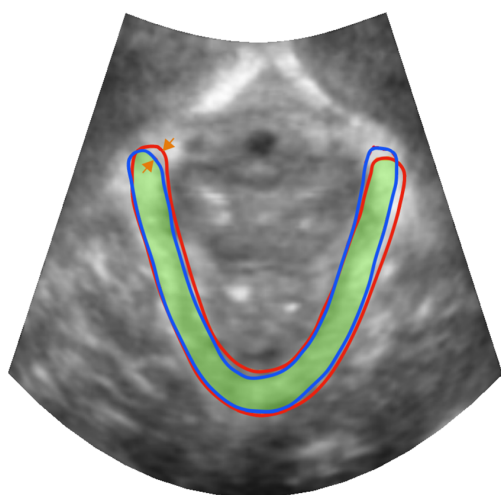


**Figure 2** Automatic (red) and manual (blue) segmentation of puborectalis muscle in slice with minimal hiatal dimensions. Arrows indicate one measurement of absolute distance between two segmentations. Green area is overlap between segmentations.

PRM data are used to train the model, it learns the natural variability in appearance of the PRM in 3D transperineal ultrasound data. In new data (not present in the training set), this model can be used to predict the position of the PRM. We used the AAM implementation described by van Stralen *et al.*<sup>16</sup>, with the leave-one-out method to train and match (finding the PRM) the AAMs, to avoid training bias in their evaluation. This means that we created 50 AAMs, using 49 manually segmented ultrasound images for the training of one AAM and the last ultrasound image for matching. Therefore, we could optimally use the manual segmentation data, both for training and as ground truth to analyze the performance of automatic segmentation.

### Validation

To validate the manual segmentation protocol, a randomly selected subset of 20 subjects had their ultrasound PRM segmented by a second observer as well as by the first observer for a second time more than a month later. This allowed for analysis of inter- and intraobserver performance. The performances of manual and automated segmentation were compared. Statistical analysis was performed using SPSS v. 23 (SPSS Inc., Chicago, IL, USA) and Excel 2011 (Microsoft Office, Microsoft Corp., Redmond, WA, USA). Means, SDs and intraclass correlation coefficients (ICCs) with their 95% CIs were used to compare MEP and volume acquired by observers and computer. ICC results were classified according to the subgroups defined by Landis and Koch<sup>22</sup>.

Although volume and MEP measurements are relevant parameters with which to analyze the performance of manual and automatic segmentation, good agreement of these does not necessarily mean good agreement in the positions of two segmentations. Therefore, we used MeVisLab to calculate three other parameters that better reflect agreement between segmentations; these were mean absolute distance (MAD), Hausdorff distance and Dice coefficient (*D*). The absolute distance is the minimum distance from one point on the segmentation to a point on the surface of the other segmentation; an example is given in Figure 2. MAD is the mean of all absolute distance measurements between two segmentations, showing on average how far apart from each other the two surfaces are. The Hausdorff distance is the maximum absolute

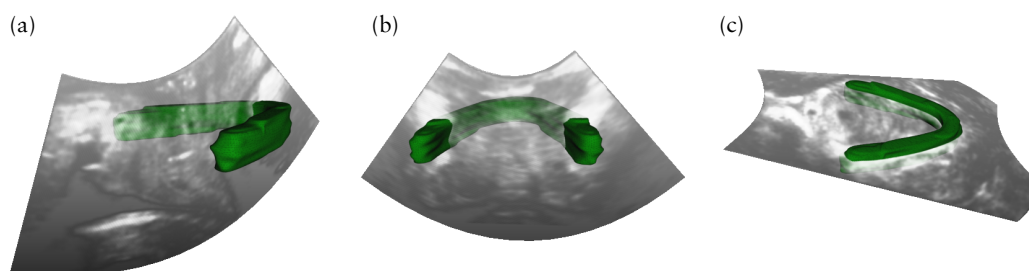


**Figure 3** Example of manual three-dimensional segmentation in transperineal ultrasound of puborectalis muscle, shown from different angles, in sagittal (a), coronal (b) and axial (c) slices.

distance between two segmentations; this gives insight into the maximum error made.  $D$  measures the overlap between segmentations, and is calculated as:

$$D = \frac{2|X \cap Y|}{|X| + |Y|}$$

where  $|X \cap Y|$  is the volume of the overlap (depicted in Figure 2 as the green area) and  $X$  and  $Y$  are the volumes of the segmentations that are being compared. If there is no overlap between segmentations,  $D$  is 0; if there is complete overlap,  $D$  is 1. Good agreement between segmentations is reflected in low MAD and Hausdorff values and in high  $D$  values.

## RESULTS

The resulting volume of a manual segmentation is shown in Figure 3. In Table 1, mean (SD) and ICCs for MEP and volume for automatic *vs* manual segmentations,

and inter- and intraobserver manual segmentations, are presented. ICCs for comparison of automatic and manual segmentations for MEP and volume were, respectively, very good and good. Inter- and intraobserver ICCs for manual segmentation showed very good agreement for both volume and MEP.

In Figure 4,  $D$ , MAD and Hausdorff distance are presented in box-and-whisker plots. The parameters that determine the distance between two segmentations, Hausdorff distance and MAD, correspond to only a few voxels mismatch. The  $D$ -values are moderate. For automatic segmentation, five mismatches were identified based on high MAD and/or low  $D$ ; these appear as outliers in Figure 4. These subjects were not included in the ICC analysis in Table 1, since measuring MEP and volume is relevant only when automatic segmentation is successful. Hausdorff distance, MAD and  $D$  show that automatic segmentation is comparable with manual segmentation if the mismatches are ignored.

**Table 1** Mean echogenicity (MEP) and volume of transperineal ultrasound three-dimensional segmentation of puborectalis muscle performed manually (by observer) *vs* automatically (by computer), manually by two independent observers and manually twice by same observer  $\geq 1$  month apart, with corresponding intraclass correlation coefficients (ICCs)

	MEP (a.u.)	ICC (95% CI)	Volume (mL)	ICC (95% CI)
Segmentation method ( $n = 45$ )				
Observer	$148 \pm 16$		$9.4 \pm 1.8$	
Computer	$147 \pm 17$	0.968 (0.941–0.982)	$9.8 \pm 2.6$	0.626 (0.327–0.794)
Interobserver ( $n = 20$ )				
Observer 1	$151 \pm 20$		$8.5 \pm 1.7$	
Observer 2	$153 \pm 18$	0.987 (0.962–0.995)	$8.6 \pm 2.1$	0.910 (0.771–0.964)
Intraobserver ( $n = 20$ )				
First set of observations	$151 \pm 20$		$8.5 \pm 1.7$	
Second set of observations	$152 \pm 19$	0.991 (0.978–0.996)	$8.8 \pm 1.7$	0.877 (0.694–0.951)

MEP and volume are given as mean  $\pm$  SD. a.u., arbitrary units.

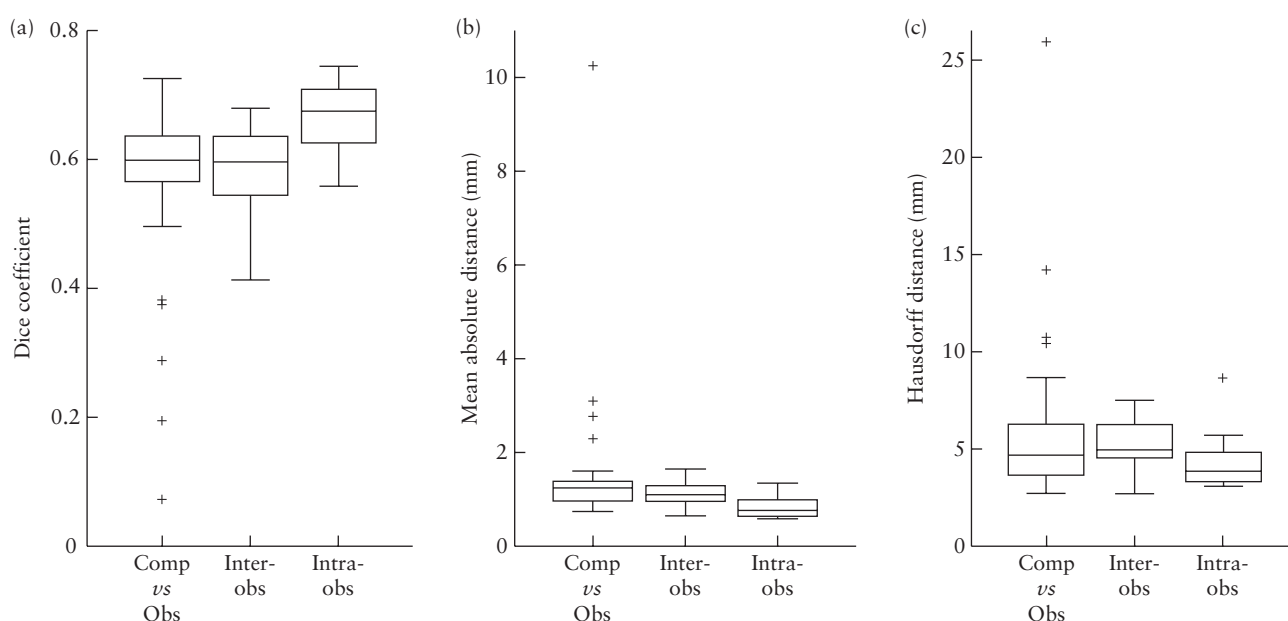


**Figure 4** Box-and-whisker plots of Dice coefficient (a), mean absolute distance (b) and Hausdorff distance (c) for computer (Comp)- *vs* observer (Obs)-derived three-dimensional segmentation of puborectalis muscle ( $n = 50$ ) and inter- and intraobserver manual segmentations ( $n = 20$ ). Boxes with internal lines represent median and interquartile range (IQR), whiskers are range excluding outliers more than  $1.5 \times$  IQR from upper and lower quartile, and + are outliers.

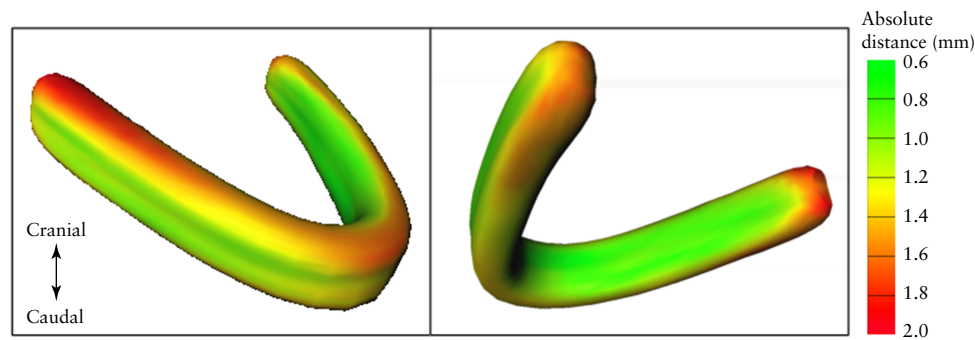


**Figure 5** Mean of manual three-dimensional segmentations of puborectalis muscle, color-coded according to average absolute distances between manual and successful automatic segmentations ( $n = 45$ ).

In Figure 5, the mean of all manual segmentations is visualized, showing average absolute distance between the manual segmentations and 45 successful automatic ones. This shows which areas are the most complicated in segmentation. These areas are the cranial and caudal limits of the PRM. Also, the site of attachment to the symphysis was found to have a high distance between manual and automatic segmentations.

## DISCUSSION

To measure 3D and 4D clinical parameters of the PRM on transperineal 3D/4D ultrasound, automatic segmentation of the PRM is needed. In this study, we present a reproducible manual segmentation protocol. AAMs trained using segmentations obtained using this protocol provided promising results for automatic segmentation, with results comparable with those of manual segmentation.

Since this is the first attempt at manual segmentation of the PRM on 3D ultrasound, the results can be compared only with segmentation results of magnetic resonance imaging or cadaver studies. The segmentation results of the PRM obtained in such studies<sup>5,23–27</sup> show very similar shapes to the those obtained in the current study, an example of which is shown in Figure 3. However, some of these studies<sup>5,24,26</sup> show that there is a thin layer of muscle fibers from other pelvic floor muscles running at the hiatal side of the PRM. These fibers are also seen in endovaginal ultrasound studies<sup>28,29</sup>. However, using endovaginal ultrasound, one is able to scan at higher frequencies to visualize the PRM, since it lies closer to the probe. On transperineal ultrasound, this layer of muscle fiber cannot be distinguished from the PRM. This does not influence the performance of automatic segmentation, but it may be of influence if this manual segmentation protocol is used for functional investigation of the PRM.

The main reason for the AAM mismatches is feces in the rectum, in which case the PRM appears darker and the feces white and the algorithm therefore segments the feces instead of the PRM. However, in 13 of the 50 images, of which only four resulted in a mismatch using the algorithm, feces can be clearly seen in the rectum. The last mismatch case was of a PRM that appeared very

dark compared with others in the training dataset. It is probable that these problems will be solved with more training data.

Hausdorff distances and MADs are comparable with the data presented by Sindhvani *et al.*<sup>15</sup> on 2D segmentation of the urogenital hiatus. The 3D-MEP ICCs are comparable with the results for 2D MEP found by Grob *et al.*<sup>12</sup>. The *D*-coefficient, however, is much lower than the values reported for 2D segmentation of the urogenital hiatus<sup>15</sup>. The first explanation for this can be found, on comparison of the 2D and 3D cases, by approximating the volume of the PRM as a cylinder ( $V = \pi r^2 h$ ) and the area of the longitudinal cross-section cylinder plane as  $A = 2rh$ , where  $r$  is radius and  $h$  is length. This shows that a mismatch in  $r$  has a larger influence on volume than on area. The second explanation is the shape of the PRM. As it is a very long and thin structure, a small shift has a much larger impact on the overlap than, for example, in the case of a spherical structure (or a 2D circle approximating the hiatus).

The strength of this study is that it provides for the first time reliable manual and automatic 3D segmentations of the PRM. This allows for measurements of MEP and volume as clinical parameters, and might be a starting point for further functional analysis. The segmentation method is based on methods that have already been proved to be reliable in 2D<sup>10–12</sup>. Since the data were obtained using a relatively old ultrasound system, even better results may be expected from data obtained using newer systems. The data were acquired using the same settings in order to measure reliably the MEP; this may have caused suboptimal image quality in certain individual cases. The application of automated 3D segmentation automates the measurement of MEP, a clinically valuable parameter<sup>13</sup>. Using the full potential of the 3D/4D nature of the data, automating the measurements in 3D will likely improve reproducibility and sensitivity, as has been shown for quantitative analyses in other domains (e.g. 2D *vs* 3D functional parameters in cardiac imaging<sup>30</sup>). Moreover, more complicated parameters, like volume, shape and function of the PRM, are now open to investigation.

Anatomical validation of our manual segmentation protocol is ongoing and further research, e.g. a cadaver study, may help us to improve the segmentation

protocol. Both automatic and manual segmentations were performed on data from subjects with an intact pelvic floor (nulliparous and at 12 weeks' gestation). The described method may perform suboptimally for data of patients with PRM trauma, since their data will have a different appearance and are not presented in the training data. The segmentation protocol may need to be updated and the training dataset of the AAM expanded with patient data. Currently, it is not possible to determine automatically if automatic segmentation was successful, e.g. for quality assurance, without the use of manual segmentation. However, in clinical practice, the physician can be the one to determine the success of automatic segmentation.

In conclusion, this study presents a reliable manual segmentation protocol for the PRM on transperineal 3D/4D ultrasound of an intact pelvic floor. Furthermore, it presents automatic segmentation of the PRM based on these data, which has results comparable with those of manual segmentation; it also allows for reliable measurement of MEP. Further studies using this method may improve our understanding of the structure and (dys-)function of the PRM.

## REFERENCES

- DeLancey JOL, Kearney R, Chou Q, Speights S, Binno S. The appearance of levator ani muscle abnormalities in magnetic resonance images after vaginal delivery. *Obstet Gynecol* 2003; **101**: 46–53.
- Dietz HP, Lanzarone V. Levator trauma after vaginal delivery. *Obstet Gynecol* 2005; **106**: 707–712.
- DeLancey JOL, Morgan DM, Fenner DE, Kearney R, Guire K, Miller JM, Hussain H, Umek W, Hsu Y, Ashton-Miller JA. Comparison of levator ani muscle defects and function in women with and without pelvic organ prolapse. *Obstet Gynecol* 2007; **109**: 295–302.
- Dietz HP, Simpson JM. Levator trauma is associated with pelvic organ prolapse. *BJOG* 2008; **115**: 979–984.
- Lien K-C, Mooney B, DeLancey JOL, Ashton-Miller JA. Levator ani muscle stretch induced by simulated vaginal birth. *Obstet Gynecol* 2004; **103**: 31–40.
- Ashton-Miller JA, Delancey JO. On the biomechanics of vaginal birth and common sequelae. *Annu Rev Biomed Eng* 2009; **11**: 163–176.
- Alperin M, Lawley DM, Esparza MC, Lieber RL. Pregnancy-induced adaptations in the intrinsic structure of rat pelvic floor muscles. *Am J Obstet Gynecol* 2015; **213**: 191.e1–7.
- Oliphant SS, Nygaard IE, Zong W, Canavan TP, Moalli PA. Maternal adaptations in preparation for parturition predict uncomplicated spontaneous delivery outcome. *Am J Obstet Gynecol* 2014; **211**: 630.e1–7.
- Grob AT, Withagen MI, van de Waarsenburg MK, Schweitzer KJ, van der Vaart CH. Changes in the mean echogenicity and area of the puborectalis muscle during pregnancy and postpartum. *Int Urogynecol J* 2016; **27**: 895–901.
- Dietz HP, Shek C, Clarke B. Biometry of the pubovisceral muscle and levator hiatus by three-dimensional pelvic floor ultrasound. *Ultrasound Obstet Gynecol* 2005; **25**: 580–585.
- Weinstein MM, Jung SA, Pretorius DH, Nager CW, den Boer DJ, Mittal RK. The reliability of puborectalis muscle measurements with 3-dimensional ultrasound imaging. *Am J Obstet Gynecol* 2007; **197**: 68.e1–6.
- Grob AT, Veen AA, Schweitzer KJ, Withagen MI, van Veelen GA, van der Vaart CH. Measuring echogenicity and area of the puborectalis muscle: method and reliability. *Ultrasound Obstet Gynecol* 2014; **44**: 481–485.
- Grob AT, Withagen MI, van de Waarsenburg MK, Schweitzer KJ, van der Vaart CH. Association of First-Trimester Echogenicity of the Puborectalis Muscle With Mode of Delivery. *Obstet Gynecol* 2016; **127**: 1021–1026.
- Grob ATM, Hitschrich N, van de Waarsenburg MK, Withagen MIJ, Schweitzer KJ, van der Vaart CH. Changes in global strain of puborectalis muscle during pregnancy and postpartum. *Ultrasound Obstet Gynecol* 2018; **51**: 537–542.
- Sindhvani N, Barbosa D, Alessandrini M, Heyde B, Dietz HP, D'Hooge J, Deprest J. Semi-automatic outlining of levator hiatus. *Ultrasound Obstet Gynecol* 2016; **48**: 98–105.
- van Stralen M, Haak A, Esther Leung KY, van Burken G, Bos C, Bosch JG. Full-cycle left ventricular segmentation and tracking in 3D echocardiography using active appearance models. *Ultrason Symp (IUS), 2015 IEEE Int.* 2015; 1–4.
- van Veelen GA, Schweitzer KJ, van der Vaart CH. Reliability of pelvic floor measurements on three- and four-dimensional ultrasound during and after first pregnancy: implications for training. *Ultrasound Obstet Gynecol* 2013; **42**: 590–595.
- Ritter F, Boskamp T, Homeyer A, Laue H, Schwier M, Link F, Peitgen HO. Medical image analysis. *IEEE Pulse* 2011; **2**: 60–70.
- Dietz HP, Bernardo MJ, Kirby A, Shek KL. Minimal criteria for the diagnosis of avulsion of the puborectalis muscle by tomographic ultrasound. *Int Urogynecol J* 2011; **22**: 699–704.
- Singh K, Jakab M, Reid WMN, Berger LA, Hoyte L. Three-dimensional magnetic resonance imaging assessment of levator ani morphologic features in different grades of prolapse. *Am J Obstet Gynecol* 2003; **188**: 910–915.
- Cootes TF, Edwards GJ, Taylor CJ. Active appearance models. *IEEE Trans Pattern Anal Mach Intell* 2001; **23**: 681–685.
- Landis JR, Koch GG. The measurement of observer agreement for categorical data. *Biometrics* 1977; **33**: 159–174.
- Feil P, Sora MC. A 3D Reconstruction Model of the Female Pelvic Floor by using plastinated cross sections. *Austin J Anat* 2014; **1**: 1022.
- Tracy PV, DeLancey JO, Ashton-Miller JA. A Geometric Capacity-Demand Analysis of Maternal Levator Muscle Stretch Required for Vaginal Delivery. *J Biomech Eng* 2016; **138**: 021001.
- Janda S, van der Helm FC, de Blok SB. Measuring morphological parameters of the pelvic floor for finite element modelling purposes. *J Biomech* 2003; **36**: 749–757.
- DeLancey JO, Sørensen HC, Lewicky-Gaupp C, Smith TM. Comparison of the puborectal muscle on MRI in women with POP and levator ani defects with those with normal support and no defect. *Int Urogynecol J* 2012; **23**: 73–77.
- Margulies RU, Hsu Y, Kearney R, Stein T, Umek WH, DeLancey JOL. Appearance of the levator ani muscle subdivisions in magnetic resonance images. *Obstet Gynecol* 2006; **107**: 1064–1069.
- Shobeiri SA, Leclaire E, Nihira MA, Quiroz LH, O'Donoghue D. Appearance of the levator ani muscle subdivisions in endovaginal three-dimensional ultrasonography. *Obstet Gynecol* 2009; **114**: 66–72.
- Rostaminia G, Peck JD, Quiroz LH, Shobeiri SA. How well can levator ani muscle morphology on 3D pelvic floor ultrasound predict the levator ani muscle function? *Int Urogynecol J* 2015; **26**: 257–262.
- Dorosz JL, Lezotte DC, Weitzenkamp DA, Allen LA, Salcedo EE. Performance of 3-dimensional echocardiography in measuring left ventricular volumes and ejection fraction: a systematic review and meta-analysis. *J Am Coll Cardiol* 2012; **59**: 1799–1808.